INSTITUTE OF PHYSICS PUBLISHING JOURNAL OF PHYSICS: CONDENSED MATTER

J. Phys.: Condens. Matter **15** (2003) 4189–4205 PII: S0953-8984(03)59860-5

Magnetic-field-induced phase transitions in Wigner molecules

B Szafran, S Bednarek and J Adamowski

Faculty of Physics and Nuclear Techniques, University of Mining and Metallurgy (AGH), al Mickiewicza 30, PL-30059 Kraków, Poland

E-mail: adamowski@ftj.agh.edu.pl

Received 21 February 2003, in final form 25 April 2003
Published 6 June 2003
Online at stacks.iop.org/JPhysCM/15/4189

Abstract

A theoretical analysis of formation and symmetry transformations is presented for Wigner molecules with $N = 2, \ldots, 20$ electrons confined in quantum dots at high magnetic fields. Using the unrestricted Hartree–Fock method with the multicentre Gaussian basis, we have found that Wigner molecules with $N \geqslant 6$ abruptly change their shape and symmetry with an associated jump in the first derivative of the ground-state energy, i.e. they undergo phase transitions. In particular, the phases of the Wigner molecules obtained just after emerging from the maximum-density droplet (MDD) phase possess a different symmetry from that formed at a high magnetic field. We show that the properties of the electron–electron interaction energy demonstrate very well both the breakdown of the MDD and the quasi-classical character of the Wigner molecule in the high magnetic field. Possible mechanisms of the MDD decay are discussed.

1. Introduction

A Wigner phase is a strongly correlated state of the electron system, in which the electrons occupy separate sites forming either a lattice (Wigner crystal) or an island-like structure (Wigner molecule). This quantum electron system with spatially separated electrons exhibits quasi-classical properties. In three-dimensional space, for a low electron density, the phase transition between the electron liquid and crystalline phases was theoretically predicted by Wigner [1]. The formation of a Wigner crystal was observed [2] in the two-dimensional (2D) electron system on the surface of liquid helium. A magnetic-field-induced liquid-to-solid phase transition was reported for a 2D electron plasma at a GaAs/GaAlAs heterojunction [3]. The existence of a pinned Wigner solid was also claimed [4] in Si at zero magnetic field, below a critical electron density. In the ground state, the 2D Wigner crystal forms a triangular (hexagonal) lattice.

Electrons confined in quantum dots (QDs) can form Wigner molecules (also called electronic molecules) [5–8]. Similar to a Wigner crystal in the absence of a magnetic field,

a Wigner molecule is created at low electron density. Application of an external magnetic field yields more favourable circumstances for the creation of a Wigner molecule [6–9]. If the magnetic field increases, the ground state of the electron system confined in the QD undergoes several transformations [10] connected with changes of the spin–orbital configurations and the shape of the electron distribution. For a sufficiently high magnetic field the electrons confined in the QD exhibit complete spin polarization [10]. In this state, called a maximum-density droplet (MDD) [8, 11, 12], the electron density distribution possesses the symmetry of the confinement potential. For a cylindrically symmetric confinement potential the electrons occupy the one-particle states with consecutive magnetic quantum numbers [11, 13]. At higher magnetic fields, the MDD phase decays. The decay of the MDD can be obtained in the framework of the mean-field approaches, i.e. the Hartree–Fock (HF) and local spin density approximation (LSDA) [8]. In the mean-field approaches, the phase that emerges from the MDD does not possess cylindrical symmetry, i.e. it corresponds to the broken-symmetry state. At very high magnetic fields the electrons occupy clearly separated islands forming a Wigner molecule [8, 11, 14]. The Wigner molecule created in the limit of an extremely high magnetic field possesses the same shape as that of a system of classical point charges [16–18]. The breakdown of the MDD has been observed in cylindrical gated QDs [19].

In the literature, different mechanisms of MDD breakdown have been reported. Reimann *et al* [11] interpreted their local-current spin-density results in terms of MDD decay beginning at the edge of the droplet. In this process, a ring of electrons separates out from a flat density maximum [11]. On the other hand, Yang and MacDonald [13] argued that the MDD phase becomes unstable when a hole appears in the electron density in the centre of the QD. In the present paper, we propose a solution to this controversy.

In a recent paper [14], we studied the possibility that Wigner molecules are formed in different space configurations (different phases) [14] and predicted the existence of several new phases of Wigner molecule. In the present paper, we provide the complete results of the calculations performed for the different Wigner molecule phases and an extensive discussion of the underlying physics. The results and discussion presented in this paper considerably extend those given in the brief announcement [14]. Moreover, we discuss the MDD breakdown mechanisms and the applicability of conditions for MDD instability. In the calculations, we have applied the unrestricted HF method with a multicentre basis, which is especially designed for the description of Wigner molecules at high magnetic fields. The proposed basis enables us to describe both the breakdown of the MDD and the quasi-classical localization of the electrons. Using this basis we have studied the behaviour of Wigner molecules with $N = 2, \ldots, 20$ electrons in the magnetic-field regime between the MDD instability and the extremely high-field classical limit.

The paper is organized as follows: section 2 contains the theoretical model and section 3 the results of the calculations of the ground-state energy and electron density distribution. In section 4, we provide a discussion and in section 5 conclusions and a summary.

2. Theory

We consider the N-electron system confined in a 2D QD and subject to an external magnetic field. We assume that the electrons are spin polarized. The magnetic field B is applied in the z direction and the electrons are confined in the x–y plane. In the effective-mass approximation, the Hamiltonian of the system has the form

$$H = \sum_{i=1}^{N}\left(h_i + V_{conf}(r_i) + \sum_{j>i}^{N}\frac{\kappa}{r_{ij}}\right) - \frac{N}{2}g^{\star}\mu_B B, \tag{1}$$

where h_i is the Hamiltonian of a single electron in the magnetic field, $\boldsymbol{r_i} = (x_i, y_i)$, $r_{ij} = |\boldsymbol{r_i} - \boldsymbol{r_j}|$, $\kappa = e^2/4\pi\varepsilon_0\varepsilon$ and ε is the static dielectric constant. The last term in equation (1) is the Zeeman energy of N spin-polarized electrons, where $g^\star$ is the effective g factor and μ_B is the Bohr magneton. The QD confinement potential is assumed to be parabolic, i.e.

$$V_{conf}(r) = \tfrac{1}{2}m\omega_0^2 r^2, \tag{2}$$

where m is the electron band mass and ω_0 is the confining frequency. In the non-symmetric (Landau) gauge, the one-particle Hamiltonian for an electron in a magnetic field has the form

$$h = -\frac{\hbar^2}{2m}\left(\frac{\partial^2}{\partial x^2} + \frac{\partial^2}{\partial y^2}\right) + \mathrm{i}\hbar\omega_c y\frac{\partial}{\partial x} + \frac{1}{2}m\omega_c^2 y^2, \tag{3}$$

where $\omega_c = eB/m$ is the cyclotron frequency,

The ground-state energy of Hamiltonian (3), i.e. the lowest Landau level, is equal to $E_0 = \hbar\omega_c/2$. Since this energy level is infinitely degenerate, we can choose the ground-state wavefunction in many forms. We have chosen [14] the one-electron ground-state wavefunction in a form of a displaced Gaussian

$$\psi_{\boldsymbol{R}}(\boldsymbol{r}) = \left(\frac{\alpha}{2\pi}\right)^{1/2}\exp[-(\alpha/4)(\boldsymbol{r} - \boldsymbol{R})^2 + (\mathrm{i}\alpha/2)(x - X)(y + Y)], \tag{4}$$

where $\boldsymbol{R} = (X, Y)$ is an arbitrary vector and $\alpha = eB/\hbar$. One can easily prove that wavefunction (4) fulfils the eigenequation for Hamiltonian (3) with eigenvalue E_0. The electron density distribution associated with wavefunction (4) has the shape of the Gaussian centred at point $\boldsymbol{R}$, which can be treated as the centre of the Landau orbit of the single electron.

In the present paper, wavefunctions (4), centred at different $\boldsymbol{R} = \boldsymbol{R}_i$, are used to form the multicentre variational basis, which is suitable for a description of Wigner molecules. A similar approach, but with the one-electron wavefunctions written in the symmetric gauge, was applied to Wigner crystals [20, 21] and Wigner molecules [22, 23]. We solve the N-electron eigenproblem by the unrestricted HF method with the one-electron wavefunctions

$$\Psi_\nu(\boldsymbol{r}) = \sum_{i=1}^{N} c_i^\nu \tilde{\psi}_{\boldsymbol{R}_i}(\boldsymbol{r}), \tag{5}$$

where ν numbers the occupied one-electron states ($\nu = 1, \ldots, N$), c_i^ν are the linear variational parameters and $\tilde{\psi}_{\boldsymbol{R}_i}(\boldsymbol{r})$ are taken in the form of (4) with the parameter α replaced by the nonlinear variational parameter $\alpha^\star$. In order to determine the positions of N centres $\boldsymbol{R}_i$ in wavefunction (5), we consider the classical counterpart of the Wigner molecule, i.e. the system of N classical equally charged particles confined in potential (2). The total potential energy of this classical system is given by

$$U_{tot}^c = \sum_{i=1}^{N}\left(V_{conf}(R_i^c) + \sum_{j>i}^{N}\frac{\kappa}{|\boldsymbol{R}_i^c - \boldsymbol{R}_j^c|}\right), \tag{6}$$

where $\boldsymbol{R}_i^c$ are the position vectors of N classical point charges in the configuration, for which potential energy (6) possesses a local minimum. In the quantum-mechanical calculations, we apply the following scaling of the centres of Gaussians: $\boldsymbol{R}_i = \sigma\boldsymbol{R}_i^c$, where the scaling factor σ is the second nonlinear variational parameter. For the sake of feasibility of the present calculations we have applied uniform scaling of the classical configurations instead of introducing separate variational parameters in the wavefunctions (5). This choice enables us to reproduce the classical configurations in the limit of the infinite magnetic field, for which the charge distribution associated with wavefunction (5) tends to that of the classical point charges.

Table 1. Ground-state energy of the 2D two-electron system in parabolic confinement for different magnetic fields B. We quote the results E_{exact} of the exact calculations, the HF estimates E_{HF}, and their difference ΔE. Energy is expressed in meV.

B (T)	E_{exact}	E_{HF}	ΔE
3	13.02	13.34	0.32
5	15.77	15.90	0.23
10	23.35	26.97	0.43
20	39.88	40.10	0.22
30	56.71	56.84	0.13

In the present paper, basis (5) contains, besides two nonlinear variational parameters $\alpha^\star$ and σ, N complex linear parameters c_i^ν for each electron, i.e. N^2 parameters for the N-electron system. However, taking into account that the linear parameters are not entirely independent, since in the HF method wavefunctions Ψ_ν are forced to be mutually orthogonal, we have at our disposal $N(N+1)/2$ independent linear variational parameters.

3. Results

Throughout the present paper, we apply the notation of different space configurations of Wigner molecules, which stems from the classical charge system [16–18]. Accordingly, we denote by N_1–N_2–N_3 the configuration of the N-electron Wigner molecule in which the inner, middle and outer shells are occupied by N_1, N_2 and N_3 electrons, respectively, whereby $N = N_1+N_2+N_3$. In the case of only two occupied shells, we label the corresponding configuration by N_1–N_2 and omit zero for the unoccupied outermost shell. This notation corresponds to the shell-like equilibrium configuration of equally charged classical particles [16–18].

In the calculations, we have used the material parameters of GaAs, i.e. $m = 0.067\ m_e$, $\varepsilon = 12.9$, $g^\star = 0.54$ and $\hbar\omega = 3$ meV. It is known that the HF method works with a relatively high precision for spin-polarized electron systems [12, 15], which are considered in the present paper. In a recent paper [14] we performed test calculations in order to check the quality of basis (5) in the high-magnetic-field regime, i.e. for $B = 20$ T. We have shown [14] that the Slater determinant constructed from wavefunctions (5) leads to the results close to the those of Müller and Koonin [6], which were obtained in a symmetric gauge with the definite angular momentum basis. For $N \geqslant 4$ the present upper bounds are better than those of [6]. We note that in our approach only one element of basis (5) is needed for each electron. Therefore, the present method requires much less computational effort than the method used in [6], in which a superposition of a large number of angular momentum eigenstates is necessary in order to reproduce the localized island-like distribution of electrons. We have also compared our results with those obtained using the Monte Carlo method [24] and found a good agreement. Moreover, we have estimated the precision of the present approach by applying it to the two-electron system with 2D parabolic confinement. In this case, the eigenproblem is separable into centre-of-mass and relative-coordinate problems, which can be solved exactly [25]. A comparison of the present HF estimates with the exact results [25] is given in table 1. The results quoted in table 1 show that the HF inaccuracy does not exceed 0.5 meV, reaches a maximum for $B = 10$ T, and then decreases with the magnetic field.

These test calculations verify the reliability of the present computational method in the magnetic-field regime considered. The high precision of the present calculations in the high-magnetic-field limit results from the fact that, in this regime, basis (5) allows us to reproduce the properties of classical Wigner molecules. However, some improvement of the present results is possible for lower magnetic fields. In order to enable the reader to verify the accuracy of the

Table 2. Energy (in meV) of the different phases of the Wigner molecules with $N = 4, 6, 9$, and 16 electrons for several values of the external magnetic field. The notation of Wigner-molecule phases is defined in the text.

B (T)	0–4	0–6	1–5	1–8	2–7	5–11	1–6–11
6	52.01	99.88	100.06	193.16	193.33	496.28	496.39
10	64.00	118.45	117.98	220.62	220.40	545.67	545.60
16	83.23	147.20	146.58	263.36	263.04	620.64	620.36
30	129.88	216.88	216.34	367.55	367.29	804.71	804.48

present approach, we list in table 2 the total energies of the 4-, 6-, 9- and 16-electron Wigner molecules in different phases.

The results for the six-electron system are displayed in figure 1, which shows the dependence of the ground-state energy on the magnetic field calculated with wavefunction (5) for the MDD and Wigner molecules in configurations 0–6 and 1–5. For the spin-polarized MDD phase the results of the restricted HF method cannot be amended by the unrestricted version of the HF method. For the MDD it is more convenient to use the symmetric gauge, since the optimal one-electron wavefunctions are the eigenstates of the single-electron operator of the z component of the angular momentum. In order to perform an additional test of the present method, we have solved the restricted HF equations by the numerical finite-difference method for the cylindrically symmetric MDD phase. This numerical approach takes into account the full cylindrical symmetry of the MDD phase and yields results that are exact within the HF approach. In figure 1, we compare these accurate results (dotted curve) with those obtained with the multicentre basis (5) (solid and dashed curves). In the MDD stability regime, the results of the calculations with the two different multicentre bases (5) slightly overestimate the exact MDD energy, but run parallel and close to the accurate curve. Moreover, both the bases, which correspond to the configurations 0–6 and 1–5, work with the same precision in the MDD regime. In the insets of figure 1, the ground-state electron density distributions are depicted. All the electron distributions, including that for the MDD phase, have been obtained with basis (5). We see that the multicentre wavefunction (5) describes the localized island-like distribution of electrons in the molecular phases and moreover reproduces surprisingly well the cylindrically symmetric electron distribution in the MDD phase.

For $B \simeq 5$ T the curves obtained with the multicentre basis (5) rapidly change their slope. Then, the charge distribution obtained with basis (5) ceases to mimic the MDD and goes over into the molecular type of localization. At this field, the energies of the 0–6 and 1–5 Wigner molecules become lower than the MDD energy. Just after the breakdown of the MDD the 0–6 phase possesses the lowest energy. However, at higher magnetic fields the 1–5 configuration becomes the lowest-energy phase. The appearance of this phase can be predicted based on the properties of the classical Wigner molecule, since the 1–5 configuration is the lowest-energy configuration of the six-electron classical Wigner molecule and the classical limit is reached at infinite magnetic field. These results indicate that the phase of the six-electron system changes first from the MDD into the 0–6 molecular phase, and next from the 0–6 into the 1–5 phase.

The determination of the critical magnetic field for MDD breakdown is rather ambiguous. In our previous paper [14] we used one possible approach, i.e. we found the magnetic field for which the energy estimate obtained with the multicentre basis becomes lower than the exact MDD energy. However, this approach overestimates the critical magnetic field, since the MDD energy is exact (within the HF method), while the upper bounds obtained with the multicentre basis (5) can be improved in the finite-magnetic-field regime. In the present paper, we also search for the critical magnetic field using another approach, which exploits only the

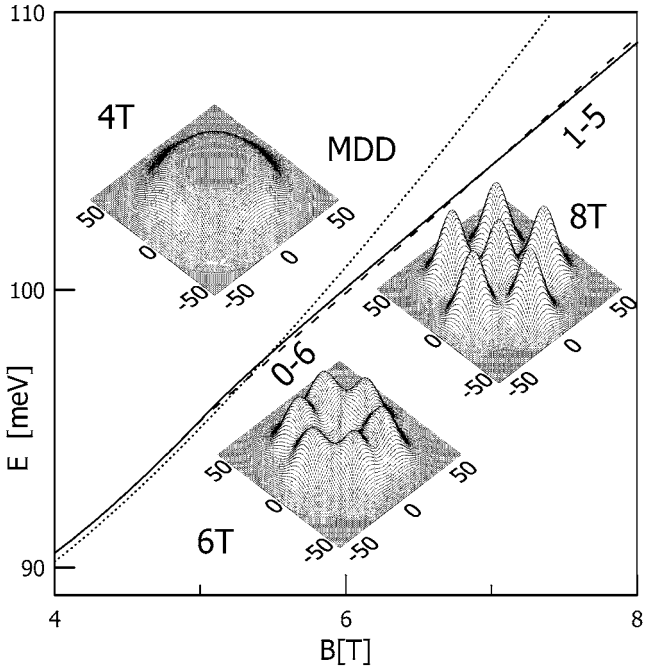

Figure 1. Ground-state energy E of the six-electron MDD (dotted curve) and the Wigner molecule in phases 0–6 (solid curve) and 1–5 (broken curve) as functions of magnetic field B. Insets show the corresponding electron density distributions on the x–y plane (length is measured in nanometres).

results obtained with basis (5). When comparing the energy estimates calculated by the same method, the possible errors cancel out, which justifies this approach. Moreover, the charge density distribution obtained with basis (5) mimics that of the MDD phase in the magnetic-field regime below the critical field for the MDD/Wigner molecule transition and yields the molecular charge distribution above the critical field.

In the present paper, instead of comparing the ground-state energies, which differ by a small amount (cf figure 1), we use the characteristic properties of the electron–electron interaction energy to extract the critical magnetic field. Figure 2 displays the expectation value of the total electron–electron interaction energy, which is defined as follows:

$$E_{int} = \langle \Phi | \sum_{i=1}^{N} \sum_{j>i}^{N} \frac{\kappa}{r_{ij}} | \Phi \rangle, \tag{7}$$

where Φ is the Slater determinant constructed from the orthogonal one-electron eigenfunctions of the HF operator obtained with basis (5). In figure 2, the magnetic-field regime to the left of the peak position corresponds to the MDD phase. The increase of the magnetic field in the MMD regime forces the electron charge distribution to shrink. As a result, in this magnetic-field regime, the electron–electron interaction increases with increasing magnetic field. At a certain magnetic field, the electron–electron repulsion becomes so strong that the MDD breaks down and the charge distribution undergoes reorganization into an island-like molecular configuration. In the molecular phase, the electron–electron interaction energy rapidly decreases. Therefore, the critical magnetic field for the breakdown of the MDD phase can be precisely determined from the position of the sharp peak on the interaction energy versus magnetic field plot (cf figure 2). The critical magnetic fields determined in such a way are equal

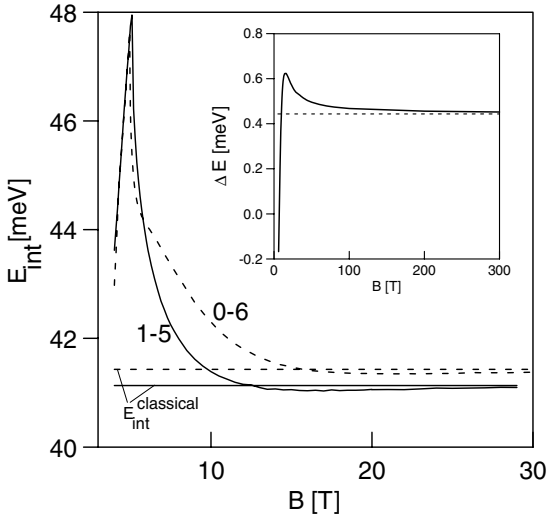

Figure 2. Expectation value E_{int} of the total electron–electron interaction energy (equation (7)) for the six-electron system confined in the QD as a function of magnetic field B. Solid (broken) curve shows the results obtained with wavefunction (5) corresponding to configuration 1–5 (0–6). The electron–electron interaction energy $E_{int}^{classical}$ is shown by the horizontal lines for classical molecules 1–5 (solid curve) and 0–6 (broken curve). Inset: energy difference ΔE between the ground-state energies of the 0–6 and 1–5 Wigner molecule phases. The horizontal broken line shows this energy difference for the classical Wigner molecule.

to 4.9 and 5.1 T, for the decay of the MDD into the 0–6 and 1–5 molecular phases respectively, which means that the 0–6 phase of the Wigner molecule is formed just after the breakdown of the MDD. The 0–6 phase has the lowest energy up to 6.95 T (cf figure 1). Above the MDD breakdown, the electron–electron interaction energies for both molecular phases decrease with increasing magnetic field, pass through flat minima and approach the corresponding high-field limit values from below. The horizontal lines in figure 2 mark the values of the electron–electron interaction energy for classical Wigner molecules (cf the second term in equation (6)). In the high-field limit, the quantum-mechanical expectation values asymptotically reach the corresponding classical values, which is another signature of the classical behaviour of the system at extremely high magnetic fields. The electron–electron interaction energy turns out to be a useful quantity for demonstrating both the MDD breakdown and the quasi-classical properties of the electrons in the high-magnetic-field limit. We have found that the plots of the interaction energy versus magnetic field B are qualitatively the same for all N.

The inset of figure 2 shows the difference ΔE of the energies of the 1–5 and 0–6 phases as a function of the magnetic field. The difference between the energies of the corresponding classical Wigner molecules is equal to 0.44 meV. We see that ΔE is maximal for $B \simeq 15$ T. At higher magnetic fields, ΔE decreases and approaches its classical limit value. The convergence to the classical value is slow and the limit is reached at infinite magnetic field.

Figure 3 shows the results for the ground-state configurations of the Wigner molecules with $N = 2, \ldots, 20$ electrons. We mark the different phases of the Wigner molecules by symbols α_i, β_i and γ_i, where α_i stands for the 0–i phase with $i = N$, β_i denotes the i–$(N - i)$ phase and γ_i denotes the phase 1–i–$(N - i - 1)$. The critical magnetic fields for the transformations between the different phases of the N-electron system confined in the QD can be found from the positions of the horizontal lines in figure 3. The uppermost horizontal solid lines show the critical magnetic fields for the formation of the Wigner molecule determined from the

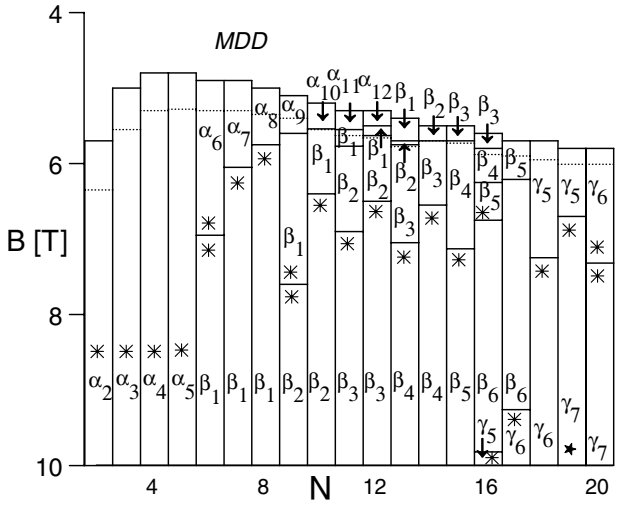

Figure 3. Phase diagram for Wigner molecules. The MDD decay and formation of different Wigner molecule phases is shown as a function of external magnetic field B and the number N of electrons. The uppermost horizontal solid lines correspond to the critical magnetic fields for the MDD decay, determined according to condition (I), described in the text. The horizontal dotted lines correspond the critical magnetic fields, determined by condition (II). The different phases of the Wigner molecules are marked by symbols α_i, β_i and γ_i, where α_i denotes the 0–i configuration with $i = N$, β_i the i–$(N-i)$ configuration, and γ_i the 1–i–$(N-i-1)$ configuration. The asterisks denote the phases for which the configuration of the Gaussian centres in basis (5) have been taken as the scaled classical configuration corresponding to the local minima of the potential energy. Other phases (without asterisks) have been obtained with the use of the additional Gaussian repulsive core (equation (8)). ($\star$) For $N = 19$ the 1–6–12 configuration becomes the ground state of the electron system at $B = 15.8$ T.

peak positions of the electron–electron interaction energy (cf figure 2), i.e. according to the condition which in the following will be referred to as condition (I). The dotted horizontal lines correspond to the values of the magnetic field for which the ground-state energy calculated with the multicentre basis becomes lower than the exact HF result for the MDD phase (cf figure 1), i.e. according to the condition which will be referred to as condition (II). In our previous paper [14] we used only condition (II) to determine the MDD breakdown. In figure 3 the following new phases, α_{10}, α_{11}, α_{12}, β_1, β_2 and β_3, appear for $N = 10, \ldots, 16$ in the range of magnetic fields for which condition (I) is fulfilled and condition (II) is not yet fulfilled. These new phases were absent in the phase diagram of [14].

The difference between the values of the critical magnetic fields determined according to conditions (I) and (II) decreases with increasing number of electrons. For example, this difference is equal to 0.7 T for $N = 2$ and 0.2 T for $N = 20$. The critical magnetic fields, determined according to condition (I) seem to be more reliable, since when applying condition (I) we are using the same method in order to estimate both the MDD and Wigner molecule energies, i.e. the errors cancel out. The critical fields derived according to condition (II) result from a comparison of the energy estimates obtained by the two different methods with different accuracies.

According to figure 3, the Wigner molecule with $N \geqslant 6$ electrons possesses at least two different ground-state configurations (phases). Each of these phases has the lowest energy in different magnetic-field regimes. For $N = 11, \ldots, 16$ electrons the Wigner molecule phase emerging from the MDD and determined by condition (I) is replaced by another phase

before condition (II) is fulfilled. The Wigner molecule phases marked by asterisks in figure 3 have been obtained using the positions of the centres of Gaussians (4) taken from the scaled classical configurations obtained with the parabolic confinement potential. Nevertheless, not all the configurations corresponding to the quantum ground state can be obtained with purely parabolic confinement. In particular, the phases which appear just after the MDD breakdown, and which correspond to the electrons gathering at the outer ring of the molecule, have to be found by another method. In order to obtain the classical configurations for these phases of the Wigner molecules, i.e. those not marked by the asterisks in figure 3, we have introduced into the confining potential a weak Gaussian repulsive core

$$U_{rep} = V_0 \sum_{i=1}^{K} \exp[-(R_i^c/R_0)^2], \tag{8}$$

which acts on a limited number K of electrons. The repulsive core (8) induces the formation of those molecules with a larger number of electrons on the outer ring. In the calculations we have used $R_0 = 30$ nm, $V_0 \in [2, 5]$ meV and $K = N$ for phases α_i, $K = N - i$ for phases β_i, and $K = N - i - 1$ for phases γ_i.

Figure 4 displays the results for the 10-electron MDD and for the 0–10, 1–9 and 2–8 phases of the Wigner molecules. The energy is calculated with respect to the energy of the 2–8 phase, which corresponds to the ground state in the high-magnetic-field limit. Crossing points (a), (b) and (c) show the values of the critical fields corresponding to the phase transitions. Point (a) corresponds to the breakdown of the MDD, obtained from condition (I). At this magnetic field, the charge densities obtained with the multicentre bases go over into the molecular-type charge densities. Above point (a), the ground-state energies, calculated with wavefunction (5) for the 0–10, 1–9 and 2–8 configurations, become different. The 0–10 configuration possesses the lowest energy up to point (b). At point (b), the ground-state energy obtained with the 0–10 and 1–9 multicentre bases crosses with the MDD energy, i.e. at this point condition (II) of the MDD breakdown is fulfilled. Moreover, the ground-state Wigner molecule changes its shape and above point (b) becomes the 1–9 configuration. Point (c) corresponds to the transition between the 1–9 and 2–8 Wigner molecule phases. The evolution of the 10-electron density distribution depicted in the insets of figure 4 indicates that the MDD decays from the centre with the formation of a hole in the electron density (cf phase 0–10). This result is compatible with the MDD breakdown mechanism proposed by Yang and MacDonald [13].

For the Wigner molecules with $N \leqslant 20$, considered in the present paper, we have found that the largest number of different phases appears for $N = 16$. According to figure 3, the 16-electron Wigner molecule can occur in five (four according to condition (II)) different phases, which are stable in different magnetic-field regimes. The energy of these phases calculated with respect to the energy of the high-field 1–5–10 phase is displayed in figure 5. The Wigner molecule occurs in phases 3–13, 4–12 and 5–11 at $B = 5.6$, 5.8 and 6.25 T respectively. We note that the transition of the 16-electron Wigner molecule into its ultimate phase 1–5–10, which corresponds to the classical equilibrium configuration, appears at particularly high magnetic field $B = 9.8$ T. This is apparently due to the fact that the classical 16-electron molecule is the one in which the third ring is formed.

Figures 6 and 7 display the electron density distributions for $N = 16$ and 20 respectively. We note that in the 1–6–13 configuration of the 20-electron Wigner molecule created just after the breakdown of the MDD (cf figure 7 for $B = 6$ T) the maxima of the electron density located on the outermost shell are much more pronounced (sharper) than those located on the inner shells. In figures 6 and 7, the contour lines introduced for $B = 6$ T correspond to the values of the charge density close to the maxima. We note that the maxima near the centre of the charge distribution are flatter and possess a larger spatial extension than those at the

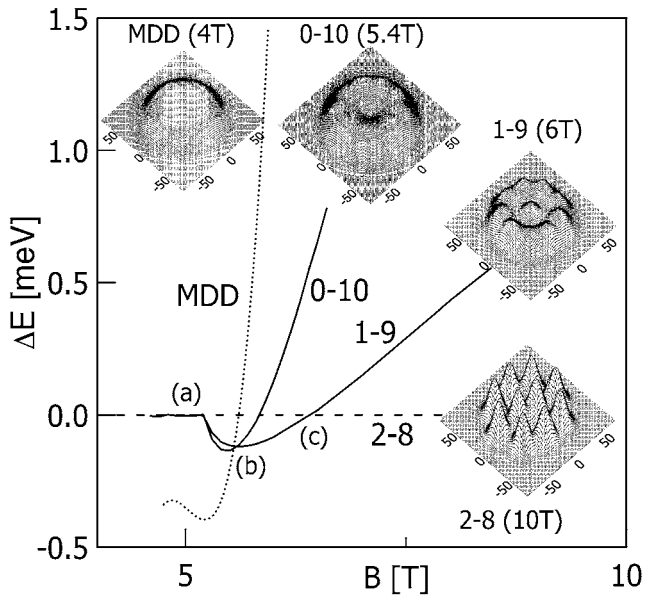

Figure 4. Energy difference ΔE between the ground-state energies of the different phases for the 10-electron system confined in the QD and the ground-state energy of the high-field 2–8 phase (broken horizontal line) as a function of magnetic field B. The dotted curve shows the results for the MDD and the solid curves show the results for the Wigner molecules in phases 0–10 and 1–9. Insets show the corresponding electron density distributions on the x–y plane (length is measured in nanometres). Points (a), (b) and (c) are described in the text.

edge. This is a trace of the MDD breakdown mechanism via edge reconstruction [11]. We will discuss this mechanism in section 4. At higher magnetic fields, all the electron density maxima are equally sharp (cf figure 7 for $B = 8$ and 12 T).

4. Discussion

The results of the present calculations show that in the external magnetic field the Wigner molecules undergo several ground-state transformations. Each of these transformations is associated with a discontinuity of the first derivative of the ground-state energy (cf figures 1, 4 and 5) and a rapid change of the spatial symmetry of the electron density distribution. Therefore, we can treat these transformations as phase transitions in a few-electron system.

We have found that a Wigner molecule with six or more electrons can appear in more than one phase. The transitions between these phases, induced by the magnetic field, exhibit a certain regularity. In the Wigner molecule phase formed from the MDD, the electrons prefer to occupy the outer shells. For $N = 6, \ldots, 12$ ($N = 6, \ldots, 10$ according to condition (II)) the molecular phases that emerge from the MDD consist of a single ring of electrons, while the quasi-classical, high-field phases are composed of two rings. However, for $N = 13, \ldots, 17$ ($N = 11, \ldots, 17$ according to condition (II)) the molecules formed from the MDD are composed of two rings, while the high-field phases consist of three rings. At higher magnetic fields, the larger number of electrons starts to occupy the inner and middle shells. In the infinite magnetic field limit, the space configuration of the electron distribution islands in the Wigner molecule exactly corresponds to the equilibrium configuration of the classical charge carriers. For finite magnetic fields, the average interelectron distances in the quantum and classical systems are different.

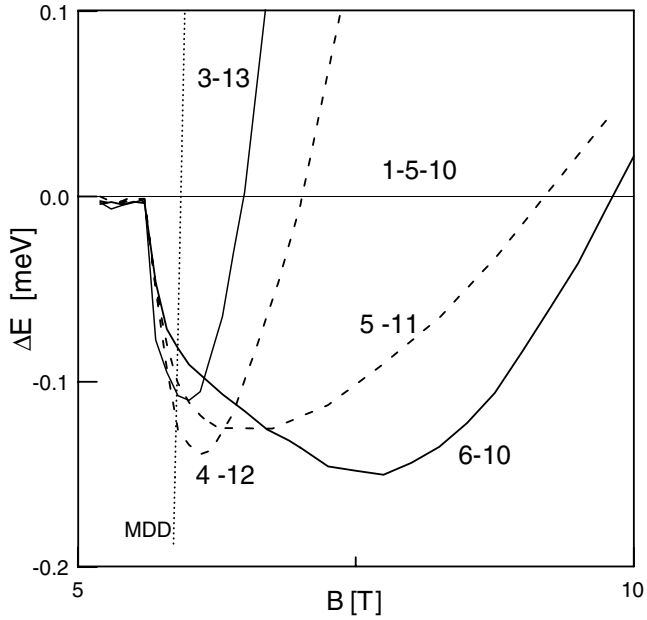

Figure 5. Energy difference ΔE between the ground-state energy of the 16-electron system confined in the QD and the ground-state energy of the high-field 1–5–10 phase (thin horizontal line) as a function of magnetic field B. The dotted curve shows the results for the MDD, the solid curves show the results for the Wigner molecule in 3–13 and 6–10 phases, and broken curves—for 4–12 and 5–11 phases.

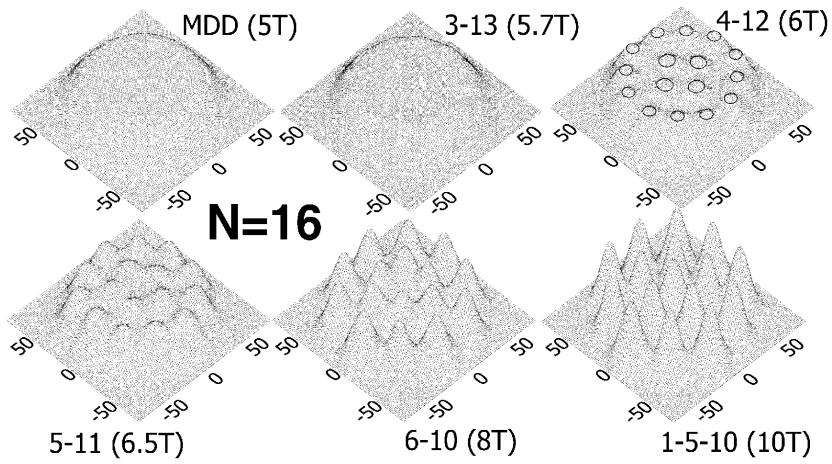

Figure 6. Electron density distribution on the x–y plane for $N = 16$ electrons for several magnetic fields. Contour lines drawn for $B = 6$ T correspond to the electron density close to the maximum. Length is measured in nanometres.

Only in the limit $B \longrightarrow \infty$ do the average interelectron distances in the quantum Wigner molecule become the same as those in the classical charge carrier system. Therefore, the application of a high magnetic field to the electron system confined in a QD allows us to observe a continuous transition from quantum mechanical to classical behaviour.

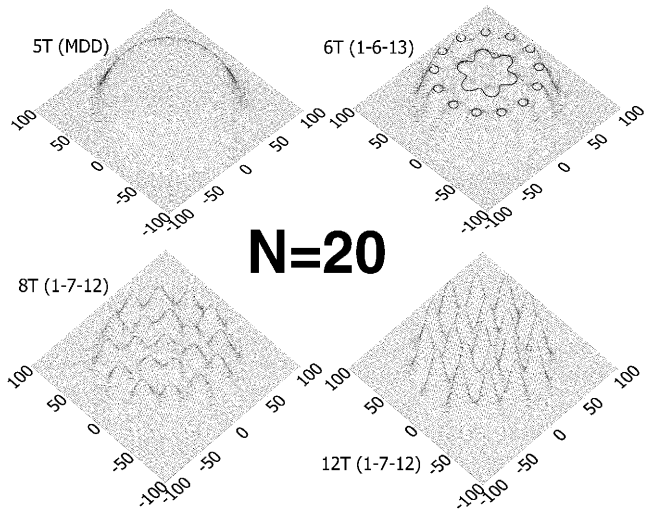

Figure 7. Electron density distribution on the x–y plane for $N = 20$ electrons for several magnetic fields. Contour lines drawn for $B = 6$ T correspond to the electron density close to the maximum. Length is measured in nanometres.

In order to get a deeper insight into the physics of Wigner molecules we have considered the different contributions to the ground-state energy. Figure 8 shows the expectation value of the Coulomb interaction energy,

$$\langle V_C \rangle = \int \mathrm{d}^2 r_1 \, \mathrm{d}^2 r_2 \, \frac{\kappa}{R} |\psi_{\boldsymbol{R}_1}(\boldsymbol{r}_1)|^2 |\psi_{\boldsymbol{R}_2}(\boldsymbol{r}_2)|^2, \tag{9}$$

calculated with ground-state wavefunctions (4) centred at $\boldsymbol{R}_1 = (0, 0)$ and $\boldsymbol{R}_2 = (0, R)$ for fixed $\alpha^\star = \alpha = eB/\hbar$ with $B = 6$ T. This energy is equal to the Hartree energy of the interaction between the two electrons with Gaussian wavefunctions (4). We notice that, contrary to the Coulomb interaction potential κ/R, the interaction energy $\langle V_C \rangle$ is non-singular at $R = 0$, i.e. the interaction energy of the two spread charges is finite, in contrast to the interaction energy of the two point charges. If the distance between the centres of two Gaussians (4) exceeds $\sim$15 nm, the Hartree energy becomes larger than κ/R. At large distances, $\langle V_C \rangle$ goes over into κ/R. In figure 8, we have also depicted the exchange integral

$$\langle E_X \rangle = \int \mathrm{d}^2 r_1 \, \mathrm{d}^2 r_2 \, \frac{\kappa}{R} \psi^*_{\boldsymbol{R}_1}(\boldsymbol{r}_1) \psi_{\boldsymbol{R}_2}(\boldsymbol{r}_1) \psi^*_{\boldsymbol{R}_2}(\boldsymbol{r}_2) \psi_{\boldsymbol{R}_1}(\boldsymbol{r}_2). \tag{10}$$

For $R = 0$ the exchange and Hartree energies take on the same values. The exchange energy rapidly decreases with R and becomes equal to zero, when the overlap between functions $\psi_{\boldsymbol{R}_1}$ and $\psi_{\boldsymbol{R}_2}$ vanishes. For $R \gtrsim 50$ nm, the two Gaussian charge distributions interact as the classical point charges. At higher magnetic fields, this effective interaction becomes classical for smaller separations between the centres of the Gaussians.

Figure 9 displays the magnetic-field dependence of the nonlinear variational parameters $\alpha^\star$ and σ in wavefunction (5) with configurations of the centres corresponding to the classical molecule (phase 1–5). Figure 9(a) shows the variational parameters in the magnetic-field regime that corresponds to the molecular phase ($B > 5.1$ T). We note that above the MDD breakdown both σ and $\alpha^\star/\alpha$ are larger than 1. In the Wigner molecules the distances between the centres of the electron localization are of the order of 30 nm. For these distances the mutual electrostatic repulsion between the Gaussian charge distributions is stronger than the repulsion

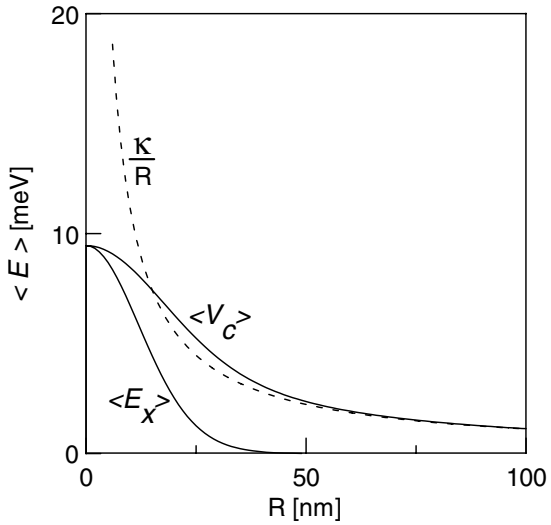

Figure 8. Expectation values of the Hartree energy $\langle V_C \rangle$ (equation (9)) and exchange energy $\langle E_X \rangle$ (equation (10)) as functions of interelectron distance R. The Coulomb interaction potential energy is shown by the dashed curve.

between point charges. Since $\sigma > 1$, the quantum Wigner molecule possesses a slightly larger size than its classical counterpart. Moreover, in the Wigner molecule $\alpha^\star > \alpha$, which means that the Gaussian charge distributions shrink as a result of the interelectron repulsion. In the magnetic-field regime, in which the transitions between different Wigner molecule phases appear, the nonlinear variational parameters deviate considerably from their high-field values (cf figure 9(a) for small B). On the other hand, in the classical high-field limit $\alpha^\star \longrightarrow \alpha$, i.e. the Gaussian electron distribution goes over into a delta-like electron localization, and $\sigma \longrightarrow 1$, i.e. the electron configuration goes over into that of the classical charge system.

Figure 9(b) shows the changes in the variational parameters in the region of the MDD/Wigner molecule phase transition. The scaling parameter σ takes on a much lower value ($\sim$0.6) for the MDD phase and rapidly jumps when the MDD decays and the molecular phase is formed. The parameter $\alpha^\star$ exhibits a small jump at the MDD/Wigner molecule phase transition.

Wavefunction (5) with the two variational parameters $\alpha^\star$ and σ is sufficiently flexible to reproduce the properties of both the MDD and molecular phases. In the present HF method, the Slater determinant is constructed from the orthogonalized wavefunctions constructed in basis (5). Kainz *et al* [22] applied the symmetric-gauge form of wavefunction (4) with only one variational parameter σ. In [22], the Slater determinant was constructed from the non-orthogonal one-electron wavefunctions. Because of this non-orthogonality, the approach of Kainz *et al* [22] is not equivalent to the HF method at finite magnetic fields. In particular, this approach [22] fails to reproduce the MDD phase, which is probably caused by the fact that every element of the Slater determinant is only one function of type (4), but not a superposition of many such functions as in the present approach. Moreover, the authors [22] found only minima of the total energy corresponding to the scaling parameter $\sigma > 1$, while in the present calculations the MDD phase is obtained if σ is much smaller than 1. In the high-field limit, orbitals (4) become orthogonal due to the lack of the overlap. Then, both the present method and the approach of Kainz *et al* [22] work with the same precision.

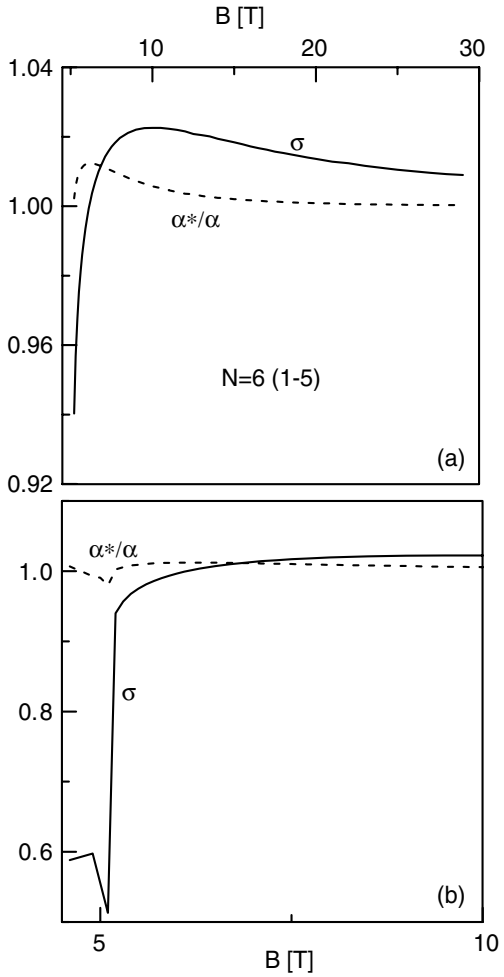

Figure 9. Nonlinear variational parameters $\alpha^\star$ and σ versus external magnetic field B for $N = 6$ obtained with the 1–5 multicentre basis. (a) The results for the Wigner molecule magnetic-field regime. (b) The results for the magnetic-field regime near the MDD breakdown.

The instability of the MDD and the formation of a broken-symmetry phase of the Wigner molecule in QDs was considered in [9, 11, 26–28]. The crossover from the Fermi liquid to the Wigner molecule behaviour was studied both in the absence [26–28] and in the presence [9, 11, 13, 29] of a magnetic field. In [9, 26–28], only a single phase of the Wigner molecule was found. Manninen *et al* [29], using an exact diagonalization scheme, found the ground state in the 0–6 configuration in the intermediate magnetic-field regime. In the present paper we have found a similar effect.

Yang and MacDonald [13] obtained a redistribution of the electrons over the orbitals with different angular momenta. They interpreted their results in terms of the holes, which arise in the occupation number distribution. The occupation number distribution [13] cannot be unambiguously translated into the spatial distribution of electrons, considered in the present paper. According to the results of [13], the decay of the MDD for $N = 2, \ldots, 14$ is accompanied by one electron missing in the zero angular momentum state, which—in terms

of the spatial electron distribution—means that the MDD decays from its centre with the electrons gathering at the outer surface. This interpretation agrees with the results of the present calculations. The results of the exact diagonalization performed by Manninen *et al* [29] for the six-electron system also confirm this mechanism of the MDD breakdown.

However, Reimann *et al* [11], based on the results of the density functional approach, suggest another mechanism for MDD breakdown via edge reconstruction [30]. According to this mechanism, the MDD undergoes a transition into the Wigner molecule gradually, when the cylindrically symmetric electron distribution of the MDD starts to break down from the edge. Then, a ring of separately localized electrons emerges from the central flat maximum of the electron distribution. The present results contradict this mechanism for $N < 12$. However, in our opinion, edge reconstruction can indeed occur for a larger number of electrons. In particular, the plots of the charge distribution presented in figures 6 and 7 indicate that during the MDD breakdown the maxima corresponding to the electrons localized at the edge of the electron distribution are sharper than the maxima corresponding to the electrons localized near the centre of the QD. Therefore, based on the present results, we suggest that the MDD starts to decay from the central part for $N \leqslant 12$ and from the edge for $N > 12$. Moreover, it is not excluded that the MDD with fewer electrons decays via simultaneous central hole formation and edge reconstruction.

Experimental evidence for the instability of the MDD phase was reported by Ooesterkamp *et al* [19]. They measured the single-electron transport through a cylindrical gated QD in a magnetic field and observed cusps on the plots, which determine the boundaries of the transport windows [10]. The conditions of the single-electron tunnelling are determined by the energy balance between the QD chemical potential (μ_N) and electrochemical potentials of the leads [10]. Since $\mu_N = E_{N+1} - E_N$, where E_N is the ground-state energy of the N-electron system confined in the QD, the cusps of the function $\mu_N(B)$ are connected with the cusps of $E_N(B)$, i.e. they result from the magnetic-field-induced phase transitions. The additional cusps were observed [19] at magnetic fields higher than those corresponding to the MDD breakdown. Based on the present results, we suggest that these additional transitions [19] can be interpreted as the phase transitions between the different phases of the Wigner molecules. A direct experimental observation of the different electron spatial localizations in the different Wigner molecule phases requires another type of measurement, e.g. wavefunction mapping [31].

5. Conclusions and summary

The present calculations have been performed under the assumption of rotational symmetry of the QD confinement potential. The mean-field approaches lead inevitably to the broken-symmetry solutions for the Wigner phase [8]. Cylindrical symmetry can be conserved by the charge distribution calculated with the exact diagonalization schemes for the Wigner phase [13, 29]. The present broken-symmetry distributions should be understood in terms of the relative electron–electron positions. The rotation of the broken-symmetry electron distribution by an arbitrary angle does not change the energy of the system. Therefore, the ground state of the Wigner molecule is infinitely degenerate with respect to the orientation. Taking this degeneracy into account, one can construct the proper ground state of the Wigner molecule as the superposition of the rotated states associated with the particular space configuration. Recently, Yannoulenas and Landman [23] have reconstructed the cylindrically symmetric solutions using a post-treatment of the broken-symmetry HF solutions obtained with a multicentre basis similar to our basis (5). If, however, the rotational symmetry of the confining potential is slightly perturbed, the orientational degeneracy of the Wigner molecule is lifted and the Wigner molecule should be pinned under a fixed angle. The pinning of

the molecule under a fixed orientation is a necessary condition for direct observation of the Wigner molecule by wavefunction mapping [31]. In real QDs, the rotational symmetry of the confinement potential can be perturbed, e.g. because of the presence of impurities near the QD region or imperfections of the nanostructure.

In summary, we have performed a systematic study of phase transitions in Wigner molecules induced by an external magnetic field. We have proposed a multicentre Gaussian basis for the N-electron system and shown that this basis is sufficiently flexible to reproduce the properties of both the MDD and the molecular phases of the electron system. The results for the MDD do not depend upon the choice of the configuration of the Gaussian centres. We have determined the critical magnetic fields for the decay of the MDD into the molecular phase. The values of these fields are different for the different phases of the Wigner molecule created. We have found that the breakdown of the MDD is accompanied by a rapid jump of the electron–electron interaction energy as a function of the magnetic field. In the magnetic-field regime above the MDD breakdown, several molecular phases possess similar energies, but the phase with the lowest energy cannot in general be identified with the lowest-energy configuration of the classical point-charge system. We have shown that with increasing magnetic field the Wigner molecule, which consists of six or more electrons, undergoes several phase transitions. In particular, we have found new phases of the Wigner molecule which differ in their spatial distribution of electrons. For comparison, the Wigner crystal, which is created in the many-electron 2D system, possesses only one equilibrium phase with fixed (triangular) symmetry. On the contrary, based on the present results we predict that the few-electron Wigner molecules created in the QDs subjected to an external magnetic field are formed in several phases with a different symmetry. We have found that a search for the cusps in the expectation value of the electron–electron interaction energy as a function of the magnetic field can be proposed as a new condition, which is suitable when determining the Wigner molecule formation from the MDD phase. We have also suggested a solution to the controversy related to the possible mechanism of the MDD/Wigner molecule transition. Based on the results of the present paper, we suggest that for $N \leqslant 12$ the MDD decays from the centre, while for $N > 12$ edge reconstruction appears.

Acknowledgment

This paper has been supported in part by the Polish Government Scientific Research Committee (KBN).

References

[1] Wigner E P 1934 *Phys. Rev.* B **46** 1002
[2] Grimes C C and Adams G 1979 *Phys. Rev. Lett.* **42** 795
[3] Andrei E Y, Deville G, Williams F I B, Paris E and Etienne B 1988 *Phys. Rev. Lett.* **60** 2765
[4] Pudalov V M, D'Iorio M, Kravchenko S V and Campbell J W 1993 *Phys. Rev. Lett.* **70** 1866
[5] Jauregui K, Haüsler W and Kramer B 1993 *Europhys. Lett.* **24** 581
[6] Müller H M and Koonin S E 1996 *Phys. Rev.* B **54** 14532
[7] Maksym P A, Imamura H, Mallon G P and Aoki H 2000 *J. Phys.: Condens. Matter* **12** R299
[8] Reimann S M and Manninen M 2002 *Rev. Mod. Phys.* **74** 2002
[9] Yannouleas C and Landman U 1999 *Phys. Rev. Lett.* **82** 5325
[10] Szafran B, Bednarek S and Adamowski J 2002 *Phys. Rev.* B **65** 35361
[11] Reimann S M, Koskinen M, Manninen M and Mottelson B R 1999 *Phys. Rev. Lett.* **83** 3270
Reimann S M, Koskinen M and Manninen M 2000 *Phys. Rev.* B **62** 8108
[12] MacDonald A H, Yang E S R and Johnson M D 1993 *Aust. J. Phys.* **46** 345
[13] Yang E S R and MacDonald A H 2002 *Phys. Rev.* B **66** 041304

[14] Szafran B, Bednarek S and Adamowski J 2003 *Phys. Rev.* B **67** 045311 (erratum 159902(E))
[15] Szafran B, Bednarek S and Adamowski J 2003 *Phys. Rev.* B **67** 115323
[16] Bolton F and Rössler U 1993 *Supperlatt. Microstruct.* **13** 139
[17] Bedanov V M and Peeters F M 1994 *Phys. Rev.* B **49** 2667
[18] Schweigert V A and Peeters F M 1995 *Phys. Rev.* B **51** 7700
[19] Oosterkamp T H, Janssen J W, Kouwenhoven L P, Austing D G, Honda T and Tarucha S 1999 *Phys. Rev. Lett.* **82** 2931
[20] Price R, Zhu X, Das Sarma S and Platzman P M 1995 *Phys. Rev.* B **51** 2017
[21] Mikhailov S A 2001 *Physica* B **299** 6
[22] Kainz J, Mikhailov S A, Wensauer A and Rössler U 2002 *Phys. Rev.* B **65** 115305
[23] Yannoulenas C and Landman U 2002 *Phys. Rev.* B **66** 115315
[24] Bolton F 1994 *Solid-State Electron.* **37** 1159
[25] Dineykhan M and Nazmitdinov R G 1999 *J. Phys.: Condens. Matter* **11** L83
[26] Egger R, Häusler W, Mak C H and Grabert H 1999 *Phys. Rev. Lett.* **82** 3320
[27] Mikhailov S A 2002 *Physica* E **12** 884
[28] Reusch B, Häusler W and Grabert H 2001 *Phys. Rev.* B **63** 113313
[29] Manninen M, Viefers S, Koskinen M and Reimann S M 2001 *Phys. Rev.* B **64** 245322
[30] Chamon C de C and Wen X G 1994 *Phys. Rev.* B **49** 8227
[31] Vdovin E E, Levin A, Patanè A, Eaves L, Main P C, Khanin Yu N, Dubrovkii Yu V, Henini M and Hill G 2000 *Science* **290** 122